Draft version January 29, 2020
Typeset using LaTeX twocolumn style in AASTeX62

WASP-4 is Accelerating Towards the Earth

L. G. Bouma,[1] J. N. Winn,[1] A. W. Howard,[2] S. B. Howell,[3] H. Isaacson,[4] H. Knutson,[5] and R. A. Matson[3]

[1] *Department of Astrophysical Sciences, Princeton University, 4 Ivy Lane, Princeton, NJ 08540, USA*
[2] *Cahill Center for Astrophysics, California Institute of Technology, Pasadena, CA 91125, USA*
[3] *NASA Ames Research Center, Moffett Field, CA 94035, USA*
[4] *Astronomy Department, University of California, Berkeley, CA 94720, USA*
[5] *Division of Geological and Planetary Sciences, California Institute of Technology, Pasadena, CA 91125, USA*

(Received January 29, 2020; Revised —; Accepted —)

Submitted to AAS journals.

ABSTRACT

Space and ground-based transit observations of the hot Jupiter WASP-4b have recently shown that its orbital period is decreasing. The period change could be caused by tidal orbital decay, orbital precession, or light-travel time effects. We present new radial velocity measurements of WASP-4, acquired with Keck-HIRES. The data show that the system is accelerating towards the Earth at $\dot{\gamma} = -0.0422^{+0.0028}_{-0.0027}\,\mathrm{m\,s^{-1}\,yr^{-1}}$. The implied period decrease probably explains WASP-4's changing orbital period as a light-travel time effect. Combining the radial velocities with new limits from speckle imaging, we find that the system's acceleration is likely caused by a 10-200 $M_{\rm Jup}$ companion with semi-major axis between 10-100 AU. The statistics from Knutson et al. (2014) imply that about 1 in 6 hot Jupiters are expected to show similar period decreases as WASP-4, due to acceleration by outer companions. We find that these period decreases will be increasingly measureable in coming years, because the precision of period derivative measurements scales as the fourth power of the observing baseline. Continued radial velocity monitoring of hot Jupiters is therefore essential to distinguish tidal orbital decay from line-of-sight accelerations.

Keywords: Exoplanet tides (497), Exoplanet dynamics (490), Radial velocity (1332), Transit timing variation method (1710)

1. INTRODUCTION

The orbits of most hot Jupiters are unstable to tidal decay (Counselman 1973; Hut 1980; Rasio et al. 1996; Levrard et al. 2009; Matsumura et al. 2010). The relevant issue is whether the timescale for tidal orbital decay is shorter or longer than the timescale for main-sequence stellar evolution. This question depends on the uncertain rate at which friction inside the star can damp the energy of tidal oscillations and thereby shrink the orbit (as reviewed by Mazeh 2008 and Ogilvie 2014).

Indirect studies of age and angular momentum indicators including the hot Jupiter semi-major axis distribution, host star spin rates, and galactic velocity dispersions have led to estimates for the inspiral timescale that vary from much less to much greater than the main-sequence evolution time (*e.g.*, Jackson et al. 2009, Teitler & Königl 2014, Penev et al. 2018, Collier Cameron & Jardine 2018, Hamer & Schlaufman 2019). Direct measurements of tidal orbital decay through transit and occultation timing could provide an empirical solution. For instance, combined transit timing and radial velocity measurements for WASP-12b have shown that its secular period decrease of ≈30 milliseconds per year is almost certainly due to tidal orbital decay (Maciejewski et al. 2016; Patra et al. 2017; Yee et al. 2020).

This study highlights a point that, though obvious, has perhaps not yet received due attention. The point is that observational programs aimed at identifying orbital decay in hot Jupiters through transit timing will be crippled without concurrent long-term radial velocity monitoring. The reason is that line-of-sight accelerations due to outer companions (*e.g.*, Agol et al. 2005) and tidal orbital decay both initially manifest identically in transit times, as a non-zero period derivative. Massive outer companions to hot Jupiters are the norm; Bryan et al. (2016) calculated an occurrence rate of $60.9^{+5.2}_{-5.6}\%$ for outer companions to hot Jupiters with masses from 1-20 $M_{\rm Jup}$ and semi-major axes from 5-100 AU. Therefore it could very well be that more hot Jupiters will show shrinking orbital periods due to long term accelerations than due to tidal orbital decay.

Corresponding author: L. G. Bouma
luke@astro.princeton.edu

The main focus of this study is the hot Jupiter WASP-4b, which has an orbital period that appears to be decreasing by about 10 milliseconds per year. We discovered the timing variations using data from TESS (Ricker et al. 2015) and a decade of ground-based observations (Bouma et al. 2019, hereafter B19). Thereafter, Southworth et al. (2019) reported 22 new transit times for the system, and found an updated decay rate of $\dot{P} = -9.2 \pm 1.1$ milliseconds per year. The Southworth et al. decay rate was $\approx 3\sigma$ less rapid than that found by B19, but the conclusions of the studies were otherwise similar. A separate study by Baluev et al. (2019) reported additional archival transit light curves of WASP-4b, most notably from TRAPPIST, and also from select other observers. Baluev et al. (2019) pointed out that when using lower-precision subsets of the available transit data, the case for a decreasing period worsened. We agree with this statement.

To determine the origin of the period change, we acquired four additional radial velocity measurements using Keck-HIRES, extending the RV baseline from 3 to 9 years. Previously, the five available HIRES radial velocities suggested a weak ($\approx 2\sigma$) linear trend (Knutson et al. 2014). Our new measurements reveal a line-of-sight acceleration of $\dot{\gamma} = -0.0422^{+0.0028}_{-0.0027}\,\mathrm{m\,s^{-1}\,yr^{-1}}$. This translates to an expected period decrease from the light-travel time effect of -5.9 milliseconds per year—about commensurate with what is observed from transits. In the following, we avoid the term "Rømer delay", which typically signifies arrival time delay due to observatory motion. We are discussing the Doppler effect seen by a stationary observer for a source with constant line-of-sight acceleration.

In the following, § 2 collects the available transit data and presents the new radial velocity and speckle imaging observations. § 3 analyzes the data, and finds that they yield a picture in which the WASP-4 system is accelerating towards our line-of-sight, likely due to the pull of a brown or M-dwarf companion. § 4 places this result in the broader context of orbital decay searches, and points out that line-of-sight accelerations, *i.e.*, "false positive orbital decay signals", are relatively common in the hot Jupiter population. § 5 offers concluding remarks.

2. OBSERVATIONS

2.1. *Transits*

Table 1 lists the transit times we collected for our analysis. We include data from the peer-reviewed literature for which *(i)* the analysis was based on observations of a single transit, *(ii)* the midpoint was fitted as a free parameter, and *(iii)* the time system specified both the leap second correction (TDB or UTC) and also whether any barycentric or heliocentric corrections had been performed.

The majority of times are identical to those we collected in B19. Twenty-two new times reported by Southworth et al. (2019) are included. These transits were observed from the 3.58m NTT and Danish 1.54m telescopes at La Silla, and the SAAO 1.0m telescope.

Additional timing measurements were also recently made available by Baluev et al. (2019), based on a homogeneous analysis of archival ground-based observations taken professional and amateur observers. We included twelve of their "high quality" transit times from TRAPPIST (six transits), El Sauce (four transits), and Petrucci et al. (2013). For TRAPPIST and El Sauce, we verified with the original observers that correct barycentric and leap-second corrections had been performed (M. Gillon, P. Evans, priv. comm.). We omitted the fourteen remaining Baluev et al. ETD[1] times due to ambiguity in whether leap-second corrections had or had not been performed.

The four available occultations tabulated by B19 have negligible statistical value due to their large uncertainties, and we forgo their use in this analysis.

2.2. *Radial velocities*

After identifying the period decrease in B19, we acquired four additional radial velocity measurements with the Keck High Resolution Echelle Spectrometer (HIRES, Vogt et al. 1994). Our observations were acquired under the purview of the California Planet Survey (Howard et al. 2010). The spectra were reduced using **software X**. Previously, the HIRES data-points spanned 2010 to 2013 (Knutson et al. 2014). Our new measurements triple the HIRES observing baseline to nine years.

The complete set of radial velocity observations is given in Table 2. Along with the 2010-2019 HIRES observations, there are also earlier measurements from CORALIE and HARPS. Following B19, we included the CORALIE measurements from Wilson et al. (2008) and Triaud et al. (2010), using the homogeneous radial velocities calculated by the latter authors. We included the HARPS values reported by Pont et al. (2011) and Husnoo et al. (2012). We omitted the HARPS data points taken over three nights by Triaud et al. (2010) for Rossiter-McLaughlin observations because they have a systematic offset from the remaining datasets.

2.3. *Speckle imaging*

A cursory analysis of the new HIRES observations led to our detection of a linear trend in the residuals after fitting out the orbit of WASP-4b. This prompted us to acquire speckle images using Zorro at Gemini-South (see Scott et al. 2018, and the instrument web-pages[2]). Zorro is a dual-channel speckle interferometer with narrow-band filters centered at 562 nm and 832 nm.

We observed WASP-4 twice, on the night of September 11-12 (8 sets of 1000 frames each) and also on the night of September 28-29 (7 sets of 1000 frames each). **We reconstructed the images following... We reduced the reconstructed speckle images to contrast curves by injecting and recovering point-sources...** The contrast curves showed that the second night, which had better seeing, also produces

[1] http://var2.astro.cz/ETD

[2] www.gemini.edu/sciops/instruments/alopeke-zorro/

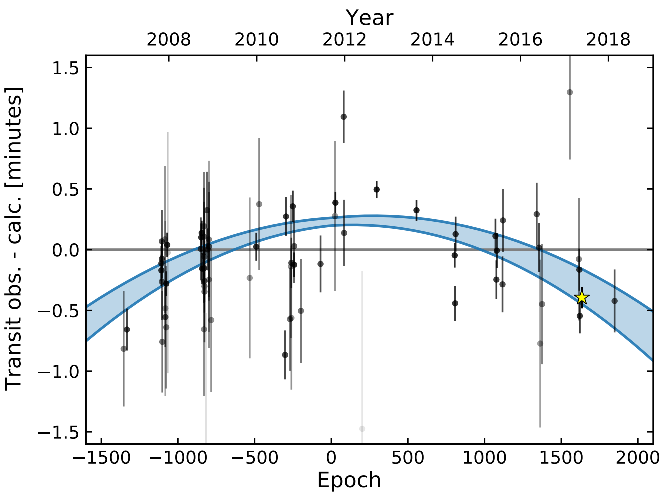

Figure 1. Timing residuals and best-fit models for WASP-4b. The vertical axis shows the observed transit times minus the calculated times assuming a constant orbital period. More opaque points correspond to more precise data. The quadratic ephemeris and its $\pm 1\sigma$ statistical uncertainties are shown in blue. Neither model fully explains the scatter in transit residuals, perhaps due to underestimated uncertainties (see 3.1). The binned TESS point (yellow star) is the weighted average of 18 TESS transits and is binned for display purposes only. Its uncertainty is slightly larger than the marker size. The models were fitted to all of the individual transit times.

the more constraining result. The 832 nm results were also typically the most constraining, since faint companions are typically redder. We therefore opt for the 832 nm September 28-29 results for the remaining analysis.

3. ANALYSIS

3.1. *Transits*

We considered two models for the observed transit times. The first model assumes a constant orbital period P on a circular orbit:

$$t_{\rm tra}(E) = t_0 + PE, \tag{1}$$

where E is the epoch number and t_0 is a reference epoch. The second model assumes that the period changes at a steady rate:

$$t_{\rm tra}(E) = t_0 + PE + \frac{1}{2}\frac{{\rm d}P}{{\rm d}E}E^2. \tag{2}$$

The free parameters are the reference epoch t_0, the period at the reference epoch P, and the period derivative, ${\rm d}P/{\rm d}t = (1/P){\rm d}P/{\rm d}E$. We defined the epoch numbers such that $E = 0$ is near the weighted average of the observed times. This helps to reduce the covariance between t_0 and P. A third possible model that we did not consider for reasons that will become apparent is a precessing, eccentric orbit (*e.g.*, Giménez & Bastero 1995; Patra et al. 2017).

We fitted each of the two models by assuming a Gaussian likelihood and sampling over the posterior probability distributions. We sampled the posterior using the algorithm proposed by Goodman & Weare (2010) and implemented by Foreman-Mackey et al. (2013) in `emcee`. The prior for the quadratic model allowed the period derivative to have any sign.

Figure 1 shows the observed transit times, minus the best-fit constant period model. The best-fitting constant-period model has 91 degrees of freedom, $\chi^2 = 276$, and $\chi^2_{\rm red} = 3.0$. The best-fitting quadratic model has 90 degrees of freedom, $\chi^2 = 183$, and $\chi^2_{\rm red} = 2.0$. The difference in the Bayesian information criteria (BIC) between the linear and quadratic and models is $\Delta{\rm BIC} = 89.1$, strongly favoring the quadratic case (Kass & Raftery 1995).

From the reduced χ^2 values, we can surmise that neither model entirely describes the transit data that we have collected—there must be some additional source of signal or noise. In Bouma et al. (2019), we found that the quadratic model for the (sparser) transit data gave $\chi^2_{\rm red} = 1.0$. The worsened $\chi^2_{\rm red}$ could reflect underestimated statistical uncertainties in any of our transit measurements. It could also reflect systematic errors in the time-systems in which the transit measurements were recorded, though we have taken every caution against this latter possibility.

One approach to analyzing such data would be to introduce a fudge factor to inflate the transit measurement uncertainties, and lower the reduced χ^2. We do not think that such an approach is warranted, since it would not change the result that the quadratic model is strongly preferred.

The best-fit period derivative in the quadratic model is

$$\dot{P} = -(2.74 \pm 0.28) \times 10^{-10} = -8.64 \pm 0.89 \ {\rm ms\,yr^{-1}}. \tag{3}$$

This agrees to within 1σ of the value reported by Southworth et al. (2019) ($\dot{P} = -9.2 \pm 1.1$ ms yr^{-1}). It is $\approx 3\sigma$ larger than the rate of period decrease we reported earlier (-12.6 ± 1.2 ms yr^{-1}; Bouma et al. 2019), presumably because of the new data from Southworth et al. and Baluev et al. The other best-fit transit timing model parameters are reported in Table 3.

3.2. *Radial Velocities: WASP-4's acceleration towards the Earth*

Our initial model for the radial velocity data was a single Keplerian orbit, plus instrument offsets, jitters, and a long-term trend (Fulton et al. 2018, `radvel`). We set Gaussian priors on the orbital period and time of inferior conjunction using the values from Table 4 of B19, and fixed WASP-4b's eccentricity to zero (Beerer et al. 2011; Knutson et al. 2014; Bonomo et al. 2017). The free parameters were the velocity semi-amplitude, the instrument zero-points, an additive "white noise" instrument jitter for each instrument, linear ($\dot{v_{\rm r}}$), and optionally second-order ($\ddot{v_{\rm r}}$) acceleration terms.

We found that the best-fitting model with both linear and quadratic radial velocity terms was marginally preferred (by $\Delta{\rm BIC} = 5.8$) over the best-fitting model with only a linear term. Regardless, for consistency with Knutson et al. (2014), who fixed the quadratic component of the long-term trend to

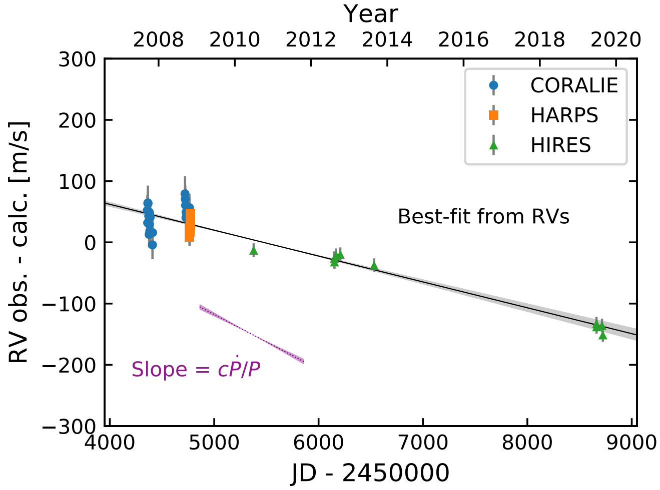

Figure 2. Radial velocity residuals of WASP-4. The best-fit Keplerian orbit of WASP-4b has been subtracted. The linear trend inferred from the RV data is shown with a black line, with 1σ errors in gray. The trend that would be needed to produce the period decrease seen in transits ($\dot{P} = -8.64 \pm 0.89$ ms yr^{-1}) is indicated with the purple dotted line. The four new RV measurements presented in this work increased the significance of the radial velocity trend from $\approx 2\sigma$ to 15σ.

zero, in Figure 2 we show best-fitting models for the linear-trend case.

WASP-4 was found to be accelerating towards our line-of-sight at high confidence,

$$\dot{v_r} = \dot{\gamma} = -0.0422^{+0.0028}_{-0.0027}\,\mathrm{m\,s^{-1}\,day^{-1}}. \quad (4)$$

For comparison, before our new measurements, $\dot{v_r}$ was thought to be about five times smaller, and was only marginally significant (Knutson et al. 2014; Bouma et al. 2019).

The system's acceleration towards our line-of-sight causes a decrease in the apparent orbital period. The period derivative expected from radial velocities is

$$\dot{P}_{\rm RV} = \frac{\dot{v_r} P}{c} = -5.94 \pm 0.39\ \mathrm{ms\,yr^{-1}}. \quad (5)$$

In other words, the majority of the period decrease observed in transits ($\dot{P} = -8.64 \pm 0.89$ ms yr^{-1}) seems to be explained by the acceleration of the host star.

An important consideration is whether the measured RV trend is correlated with stellar activity. We investigate this by analyzing WASP-4's emission in the Ca II H & K lines, as quantified with the chromospheric S-index (Wright et al. 2004). We only examined the HIRES velocities for this step, since they are the main source of signal for our analysis. First, we subtracted the orbital solution from the Keck-HIRES velocities. Then, following Bryan et al. (2016, 2019), we calculated the Spearman rank correlation coefficient between the S-index and the orbit-subtracted velocities. We found a correlation coefficient of 0.16. This correlation is not statistically significant; the corresponding p-value is 0.65.

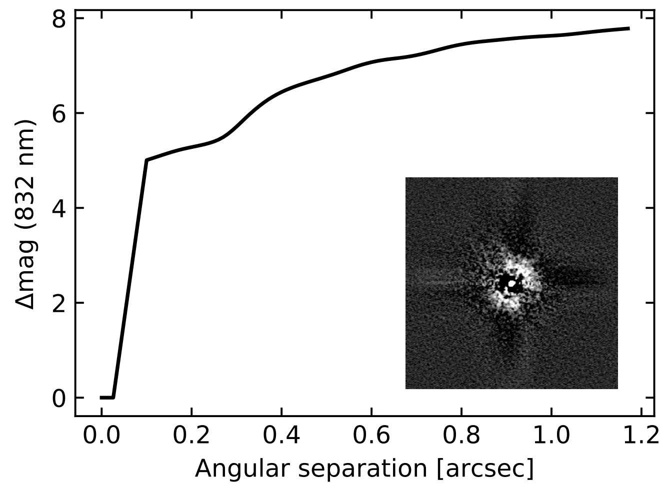

Figure 3. Zorro contrast curve derived from point-source injection-recovery experiments. Sources below the curve would have been detected. The inset shows the speckle image reconstructed from 1000 40 millisecond frames in an 832 nm bandpass, and acquired on September 28, 2019. The image scale is $2.46'' \times 2.46''$.

Furthermore, inspection of the S-index timeseries did not show secular or sinusoidal trends, as would be expected if we were observing a long-term magnetic activity cycle. The S-index values are included in Table 2. We conclude that it is highly unlikely that the linear trend is caused by stellar activity.

3.3. *Constraints on companion masses and semi-major axes*

Given a linear radial velocity trend, we can place lower-limits on the mass and semi-major axis of additional bodies in the system. As a quick estimate of the minimum mass required to explain the linear trend in WASP-4, we turn to Feng et al. (2015). As they discuss, the scenario that yields the minimum companion mass for a system with a linear trend is a companion with $e \approx 0.5$ and $\omega = 90°$. From their Equation 1,

$$M_{\rm min} \approx 0.0164\, M_{\rm Jup} \left(\frac{\tau}{\rm yr}\right)^{4/3} \left|\frac{\dot{\gamma}}{\rm m\,s^{-1}\,yr^{-1}}\right| \left(\frac{M_\star}{M_\odot}\right)^{2/3}, \quad (6)$$

where τ is the observing baseline. For WASP-4, this yields $M_{\rm min} = 4.7 M_{\rm Jup}$. Higher masses are allowed for companions that orbit further from the star: at fixed $\dot{\gamma}$, $M_{\rm comp} \propto a^2$ (Torres 1999; Liu et al. 2002).

High-resolution images can further limit the available parameter space by setting an upper limit on the semimajor axis, and a maximum brightness (and thereby mass) of any putative companions. The procedure we use to combine constraints from both radial velocities and high resolution imaging has been developed by Wright et al. (2007), Crepp et al. (2012), Montet et al. (2014), Knutson et al. (2014), Bryan et al. (2016, 2019), and others.

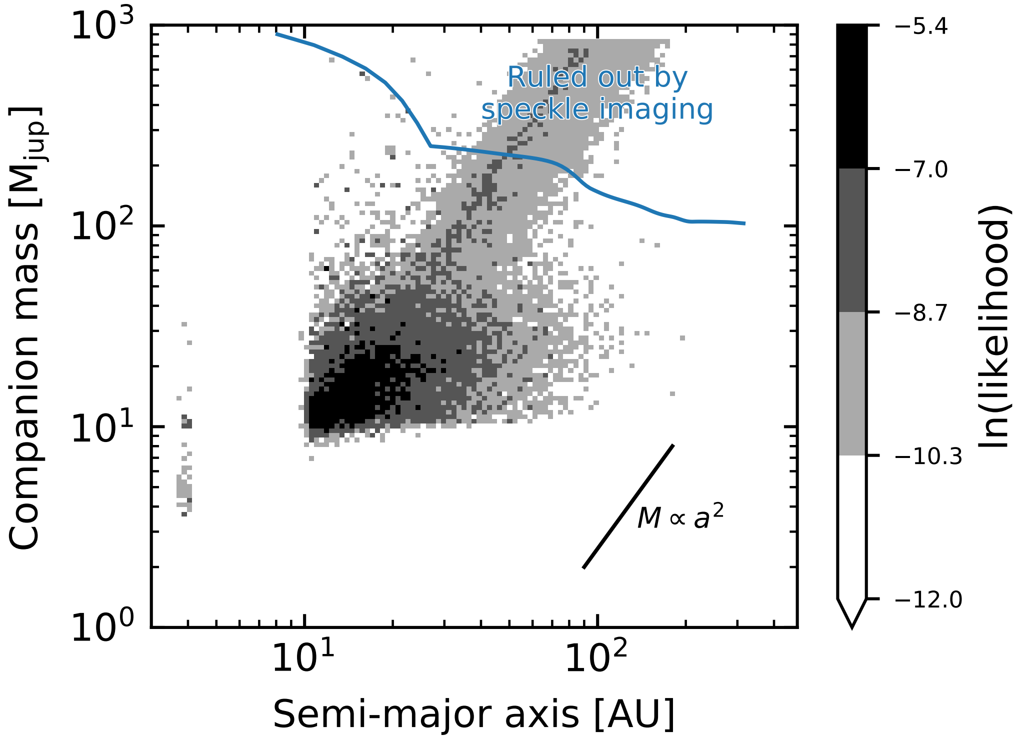

Figure 4. Masses and semi-major axes of companions that meet requirements of both the radial velocity and the speckle imaging. The likelihood inferred from radial velocities is shown in grayscale, and the region excluded from the speckle imaging is indicated (blue line). The expected mass to semimajor-axis degeneracy is shown with a black line.

Speckle imaging constraints —First, we would like to convert the contrast ratios obtained through the Zorro imaging (Figure 3) to limits on the masses of putative companions and their separations from the host star.

To do this, we followed Montet et al. (2014), and opted to employ the Baraffe et al. (2003) models for substellar mass objects and the MIST isochrones for stellar mass objects (Paxton et al. 2011, 2013, 2015; Dotter 2016; Choi et al. 2016). We assumed that the system age was 5 Gyr, so that companions would have fully contracted.

Due to the custom filters of the Zorro imager, and corresponding lack of synthetic photometry, we further assumed that all sources had blackbody spectra. While this is a bold simplification, we do not readily have access to the planetary and stellar atmosphere models needed for the consistent calculation with the `COND03` and `MESA` models. We therefore adopted the effective temperatures and bolometric luminosities from the Baraffe et al. (2003) and MIST isochrones. Using these theoretical quantities and the empirically-measured Zorro bandpasses, we calculated absolute magnitudes in the 562 and 832 nm Zorro bands for stellar and planetary mass companions. Applying the same calculation to WASP-4 itself using the effective temperature and bolometric luminosity from B19, we derived the transformation from contrast ratio to companion mass. The resulting limits are shown in Figure 4.

Radial velocity constraints —To derive constraints on possible companion masses and separations from the radial velocities, we mostly followed the procedure of Bryan et al. (2019).

We began by defining a 128×128 grid in true planetary mass and semimajor axis, with even logarithmic spacing from 1 to $900\,M_{\rm Jup}$ and 3 to 500 AU. We then considered the possibility that an additional companion in any particular cell could explain the observed linear trend. In each cell, we simulated 512 hypothetical companions.

We assigned each companion a mass and semimajor axis from log-uniform distributions within the grid cell. We drew the inclination from a uniform distribution in $\cos i$. For companion masses less than $10\,M_{\rm Jup}$, we drew the eccentricity from Kipping (2013)'s long-period exoplanet Beta distribution ($a = 1.12$, $b = 3.09$). If the companion mass exceeded $10\,M_{\rm Jup}$, we drew the eccentricity distribution from the power-law $p_e \propto e^{\eta}$ reported by Moe & Stefano (2017) in their Equation 17. We emphasize that the long-period exoplanet and long-period binary eccentricity distributions are quite different: the exoplanet distribution is "bottom-heavy", with eccentricities preferentially close to zero. The binary star distribution is "top-heavy", with eccentricities closer to one. We chose a mass cutoff of $10\,M_{\rm Jup}$ to separate the two regimes based on the bound observed by Schlaufman (2018) between giant planets and brown dwarfs, though this value is also close to the $13\,M$Jup required for a solar-metallicity body to significantly burn deuterium (Burrows et al. 1997).

For each simulated companion, we then drew a sample from the converged chains of our initial model of WASP-4b. We subtracted the planet's orbital solution, leaving RV points with a linear trend. Given (a_c, M_c, e_c) for each simulated outer companion, and the fixed instrument offsets and jitters from the MCMC chains, we then performed a maximum likelihood fit for the time and argument of periastron of the outer simulated companion. We converted the resulting $128 \times 128 \times 512$ cube of log-likelihood values to probabilities, and averaged over the samples in each grid cell to derive a probability distribution in mass and semi-major axis. Figure 4 shows the result.

4. DISCUSSION

4.1. *Implications for WASP-4*

Previous potential explanations for WASP-4b's decreasing orbital period included tidal orbital decay, orbital precession, and light-travel time effects (Bouma et al. 2019). Our new radial velocity measurements strongly indicate that the least exotic option—light-travel time effects—is also the most likely. Transits show the obital period decreasing by -8.64 ± 0.89 ms yr^{-1}; the line-of-sight acceleration observed in radial velocities would predict a period decrease of -5.94 ± 0.39 ms yr^{-1}. Though the quantitative agreement is not perfect, Occam's razor would suggest that the line of sight acceleration is probably a sufficient explanation for the apparent decrease of WASP-4b's orbital period.

The corresponding requirements for the companion causing the acceleration are that it is likely either a brown-dwarf or low mass star, orbiting between 10-100 AU from the host star (Figure 4). Given such a mass, this companion could at one time have influenced the orbital evolution of the inner giant. The fact that most hot Jupiters have similar massive outer companions (Knutson et al. 2014; Bryan et al. 2016) is circumstantial evidence for certain high-eccentricity formation channels (see Dawson & Johnson 2018). Further radial velocity monitoring should eventually reveal the orbital parameters and minimum mass of WASP-4's companion.

4.2. *How many other hot Jupiters are accelerating towards the Earth?*

We identified WASP-4b's decreasing orbital period as part of a search for tidal orbital decay. However, most hot Jupiters have companions outside of 5 AU with super-Jovian masses (Knutson et al. 2014; Bryan et al. 2016). Line-of-sight accelerations are correspondingly common in hot Jupiter systems.

To evaluate the importance of these effects for future transit timing analyses, we collected the linear radial velocity trends reported by Knutson et al. (2014), and computed the expected orbital period derivatives $\dot{P}_{\rm RV} = \dot{v}_r P/c$ for each system. The results are given in Table 4, and visualized for hot Jupiters with significant ($>3\sigma$) linear trends in Figure 5.

Including WASP-4b, 16 of 51 hot Jupiters surveyed by Knutson et al. (2014) show a non-zero radial velocity trend. Therefore around 1 in 3 hot Jupiters is expected to show period changes commensurate with WASP-4 due to acceleration by outer companions. Half of these will be period decreases, and will be an astrophysical false positive in searches for tidal orbital decay.

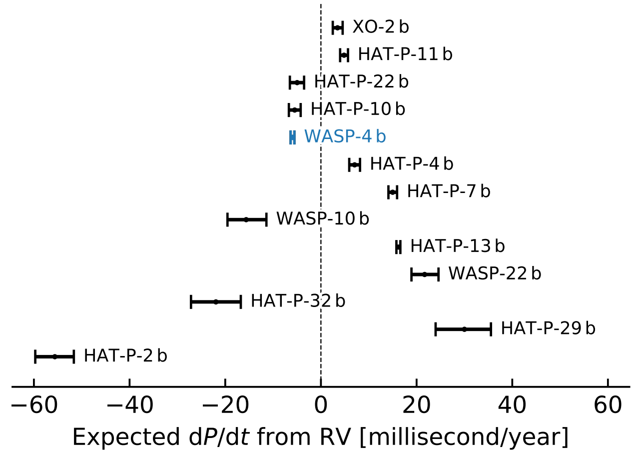

Figure 5. Predicted hot Jupiter period changes from linear radial velocity trends. Including WASP-4b, 16 of 51 hot Jupiters from Knutson et al. (2014) have shown long-term radial velocity trends. The HAT-P-11 signal is plotted, though its radial velocity signal may be caused by stellar activity. Three hot Jupiters are not plotted because their radial velocity curves better described as quadratic trends in time: HAT-P-17, WASP-8, and WASP-34. Objects are ordered in the y dimension by the absolute value of dP/dt.

4.3. *At what rate is the measurement precision of dP/dt increasing?*

For hot Jupiters that have been monitored for over baselines of $\approx$10 years, secular changes in their orbital periods are currently being constrained to a precision of $\lesssim 10$ ms yr^{-1} (*e.g.*, K. Patra et al. 2020, submitted). This is roughly commensurate with the level of signal many outer companions are expected to induce (Figure 5).

It is therefore pertinent to ask at what point in time further detections of the light-travel time effect will become routine for hot Jupiters. This question is the same as asking: at what rate does the uncertainty in the quadratic term of Equation 2 scale with the observing baseline? We take a Fisher analysis approach to the problem. First, we rewrite Equation 2 as

$$t_{\rm tra} = a_0 + a_1 E + a_2 E^2, \tag{7}$$

where $a_0 \equiv t_0$, $a_1 \equiv P$, and $a_2 \equiv 0.5 \cdot dP/dE$. By following Gould (2003), we derived that if N transit timing measurements are taken uniformly across a baseline of ΔE epochs with constant precision $\sigma_{\rm tra}$, then the uncertainty of the quadratic term is given by

$$\sigma_{a_2} = \left(\frac{25{,}920}{N}\right)^{1/2} \frac{\sigma_{\rm tra}}{(\Delta E)^4} \tag{8}$$

This result implies that a doubled observing baseline yields a sixteen-fold improvement in precision on dP/dt. If regular observations continue from ground and space-based observatories, period derivatives with precision below 1 ms yr^{-1} will be measureable before 2030.

5. CONCLUSIONS

From newly acquired radial velocity measurements, we found that WASP-4 is accelerating towards the Earth at $\dot{\gamma} = -0.0422^{+0.0028}_{-0.0027}$ $\mathrm{m\,s^{-1}\,yr^{-1}}$. The corresponding light-travel time effect predicts a period decrease $\dot{\gamma}P/c$ of -5.94 ± 0.39 $\mathrm{ms\,yr^{-1}}$. The majority of the period decrease observed in transits ($\dot{P} = -8.64 \pm 0.89$ $\mathrm{ms\,yr^{-1}}$) is therefore explained by the acceleration of the host star — not tidal orbital decay, or apsidal precession. The companion causing the acceleration is most likely a brown dwarf or low-mass star with semi-major axis between 10-100 AU.

Most hot Jupiters have outer companions with masses larger than Jupiter beyond 5 AU (Knutson et al. 2014; Bryan et al. 2016). The accelerations and period changes induced by these outer companions will become an increasingly large nuisance in the hunt for orbital decay as the observational baselines get longer. In particular, the precision with which the period derivative can be measured from transits scales as the fourth power of the baseline duration (§ 4.3), and so within a decade many more hot Jupiters should show orbital period changes due to accelerations induced by their outer companions. This effect can be distinguished from tidal orbital decay through long-term radial velocity monitoring of hot Jupiters.

Software: `astrobase` (Bhatti et al. 2018), `astropy` (Astropy Collaboration et al. 2018), `astroquery` (Ginsburg et al. 2018), `corner` (Foreman-Mackey 2016), `emcee` (Foreman-Mackey et al. 2013), `IPython` (Pérez & Granger 2007), `matplotlib` (Hunter 2007), `MESA` (Paxton et al. 2011, 2013, 2015) `numpy` (Walt et al. 2011), `pandas` (McKinney 2010), `radvel` (Fulton et al. 2018), `scipy` (Jones et al. 2001).

REFERENCES

Agol, E., Steffen, J., Sari, R., & Clarkson, W. 2005, MNRAS, 359, 567

Astropy Collaboration, Price-Whelan, A. M., Sipőcz, B. M., et al. 2018, AJ, 156, 123

Baluev, R. V., Sokov, E. N., Jones, H. R. A., et al. 2019, MNRAS, 490, 1294

Baraffe, I., Chabrier, G., Barman, T. S., Allard, F., & Hauschildt, P. H. 2003, A&A, 402, 701

Beerer, I. M., Knutson, H. A., Burrows, A., et al. 2011, ApJ, 727, 23

Bhatti, W., Bouma, L. G., & Wallace, J. 2018, `astrobase`, https://doi.org/10.5281/zenodo.1469822

Bonomo, A. S., Desidera, S., Benatti, S., et al. 2017, A&A, 602, A107

Bouma, L. G., Winn, J. N., Baxter, C., et al. 2019, AJ, 157, 217

Bryan, M. L., Knutson, H. A., Lee, E. J., et al. 2019, AJ, 157, 52

Bryan, M. L., Knutson, H. A., Howard, A. W., et al. 2016, ApJ, 821, 89

Burrows, A., Marley, M., Hubbard, W. B., et al. 1997, ApJ, 491, 856

Choi, J., Dotter, A., Conroy, C., et al. 2016, ApJ, 823, 102

Collier Cameron, A., & Jardine, M. 2018, MNRAS, 476, 2542

Counselman, C. C. 1973, ApJ, 180, 307

Crepp, J. R., Johnson, J. A., Howard, A. W., et al. 2012, ApJ, 761, 39

Dawson, R. I., & Johnson, J. A. 2018, ARA&A, 56, 175

Dotter, A. 2016, ApJS, 222, 8

Dragomir, D., Kane, S. R., Pilyavsky, G., et al. 2011, AJ, 142, 115

Feng, Y. K., Wright, J. T., Nelson, B., et al. 2015, ApJ, 800, 22

Foreman-Mackey, D. 2016, The Journal of Open Source Software, 24

Foreman-Mackey, D., Hogg, D. W., Lang, D., & Goodman, J. 2013, PASP, 125, 306

Fulton, B. J., Petigura, E. A., Blunt, S., & Sinukoff, E. 2018, PASP, 130, 044504

Gillon, M., Smalley, B., Hebb, L., et al. 2009, A&A, 496, 259

Giménez, A., & Bastero, M. 1995, Ap&SS, 226, 99

Ginsburg, A., Sipocz, B., Madhura Parikh, et al. 2018, Astropy/Astroquery: V0.3.7 Release

Goodman, J., & Weare, J. 2010, Communications in Applied Mathematics and Computational Science, 5, 65

Gould, A. 2003, arXiv Astrophysics e-prints, arXiv:astro–ph/0310577

Hamer, J. H., & Schlaufman, K. C. 2019, AJ, 158, 190

Howard, A. W., Johnson, J. A., Marcy, G. W., et al. 2010, ApJ, 721, 1467

Hoyer, S., López-Morales, M., Rojo, P., et al. 2013, MNRAS, 434, 46

Huitson, C. M., Désert, J.-M., Bean, J. L., et al. 2017, AJ, 154, 95

Hunter, J. D. 2007, Computing in Science & Engineering, 9, 90

Husnoo, N., Pont, F., Mazeh, T., et al. 2012, MNRAS, 422, 3151

Hut, P. 1980, A&A, 92, 167

Jackson, B., Barnes, R., & Greenberg, R. 2009, ApJ, 698, 1357

Jones, E., Oliphant, T., Peterson, P., et al. 2001, Open source scientific tools for Python

Kass, R. E., & Raftery, A. E. 1995, Journal of the American Statistical Association, 90, 773

Kipping, D. M. 2013, MNRAS:l, 434, L51

Knutson, H. A., Fulton, B. J., Montet, B. T., et al. 2014, ApJ, 785, 126

Levrard, B., Winisdoerffer, C., & Chabrier, G. 2009, ApJ, 692, L9

Liu, M. C., Fischer, D. A., Graham, J. R., et al. 2002, ApJ, 571, 519

Maciejewski, G., Dimitrov, D., Fernández, M., et al. 2016, A&A, 588, L6

Matsumura, S., Peale, S. J., & Rasio, F. A. 2010, ApJ, 725, 1995

Mazeh, T. 2008, in EAS Publications Series, Vol. 29, EAS Publications Series, ed. M.-J. Goupil & J.-P. Zahn, 1

McKinney, W. 2010, in Proceedings of the 9th Python in Science Conference, ed. S. van der Walt & J. Millman, 51

Moe, M., & Stefano, R. D. 2017, ApJS, 230, 15

Montet, B. T., Crepp, J. R., Johnson, J. A., Howard, A. W., & Marcy, G. W. 2014, ApJ, 781, 28

Nikolov, N., Henning, T., Koppenhoefer, J., et al. 2012, A&A, 539, A159

Ogilvie, G. I. 2014, ARA&A, 52, 171

Patra, K. C., Winn, J. N., Holman, M. J., et al. 2017, AJ, 154, 4

Paxton, B., Bildsten, L., Dotter, A., et al. 2011, ApJS, 192, 3

Paxton, B., Cantiello, M., Arras, P., et al. 2013, ApJS, 208, 4

Paxton, B., Marchant, P., Schwab, J., et al. 2015, ApJS, 220, 15

Penev, K., Bouma, L. G., Winn, J. N., & Hartman, J. D. 2018, AJ, 155, 165

Pérez, F., & Granger, B. E. 2007, Computing in Science and Engineering, 9, 21

Petrucci, R., Jofré, E., Schwartz, M., et al. 2013, ApJL, 779, L23

Pont, F., Husnoo, N., Mazeh, T., & Fabrycky, D. 2011, MNRAS, 414, 1278

Ranjan, S., Charbonneau, D., Désert, J.-M., et al. 2014, ApJ, 785, 148

Rasio, F. A., Tout, C. A., Lubow, S. H., & Livio, M. 1996, ApJ, 470, 1187

Ricker, G. R., Winn, J. N., Vanderspek, R., et al. 2015, Journal of Astronomical Telescopes, Instruments, and Systems, 1, 014003

Sanchis-Ojeda, R., Winn, J. N., Holman, M. J., et al. 2011, ApJ, 733, 127

Schlaufman, K. C. 2018, ApJ, 853, 37

Scott, N. J., Howell, S. B., Horch, E. P., & Everett, M. E. 2018, PASP, 130, 054502

Southworth, J., Hinse, T. C., Jørgensen, U. G., et al. 2009, MNRAS, 396, 1023

Southworth, J., Dominik, M., JÃÿrgensen, U. G., et al. 2019, MNRAS, 490, 4230

Teitler, S., & Königl, A. 2014, ApJ, 786, 139

Torres, G. 1999, PASP, 111, 169

Triaud, A. H. M. J., Collier Cameron, A., Queloz, D., et al. 2010, A&A, 524, A25

Urban, S., & Seidelmann, P. 2012, Explanatory Supplement to the Astronomical Almanac (University Science Books)

Vogt, S. S., Allen, S. L., Bigelow, B. C., et al. 1994, SPIE Conference Series, ed. D. L. Crawford & E. R. Craine, Vol. 2198

Walt, S. v. d., Colbert, S. C., & Varoquaux, G. 2011, Computing in Science & Engineering, 13, 22

Wilson, D. M., Gillon, M., Hellier, C., et al. 2008, ApJL, 675, L113

Winn, J. N., Holman, M. J., Carter, J. A., et al. 2009, AJ, 137, 3826

Wright, J. T., Marcy, G. W., Butler, R. P., & Vogt, S. S. 2004, ApJS, 152, 261

Wright, J. T., Marcy, G. W., Fischer, D. A., et al. 2007, ApJ, 657, 533

Yee, S. W., Winn, J. N., Knutson, H. A., et al. 2020, ApJL, 888, L5

Table 1. WASP-4b transit times.

t_{tra} [BJD$_{\mathrm{TDB}}$]	$\sigma_{t_{\mathrm{tra}}}$ [days]	Epoch	Time Reference	Observation Reference
2454368.59279	0.00033	-1354	Hoyer et al. (2013)	Wilson et al. (2008)
2454396.69576	0.00012	-1333	Hoyer et al. (2013)	Gillon et al. (2009)
2454697.79817	0.00009	-1108	Hoyer et al. (2013)	Winn et al. (2009)
2454701.81303	0.00018	-1105	Hoyer et al. (2013)	Hoyer et al. (2013)

NOTE— Table 1 is published in its entirety in a machine-readable format. Four rows are shown for guidance regarding form and content. t_{tra} is the measured transit midtime, and $\sigma_{t_{\mathrm{tra}}}$ is its 1σ uncertainty. "Time Reference" refers to the provenance of the timing measurement, which may differ from the "Observation Reference" in cases for which a homogeneous timing analysis was performed. The Hoyer et al. 2013 BJD$_{\mathrm{TT}}$ times are equal to BJD$_{\mathrm{TDB}}$ for our purposes (Urban & Seidelmann 2012). We omitted the timing measurements from Southworth et al. (2009), since there were technical problems with the computer clock at the time of observation (Nikolov et al. 2012). The two Baxter et al. (in prep) times were obtained from Spitzer/IRAC transit light curves in the 3.6μm and 4.5μm channels.

Table 2. WASP-4b radial velocities.

Time [BJD$_{\mathrm{TDB}}$]	RV [m s^{-1}]	σ_{RV} [m s^{-1}]	S-value	Instrument	Provenance
2454321.12345	42	0.42	0.42	HIRES	Knutson et al. (2014)

NOTE— Table 2 is published in its entirety in a machine-readable format. The first few entries are shown for guidance regarding form and content. S-values are collected only for the HIRES measurements.

Table 3. Best-fit transit timing model parameters.

Parameter	Median Value (Unc.)[a]
Constant period	
t_0 [BJD$_{\mathrm{TBD}}$]	2456180.558712(+14)(-14)
P [days]	1.338231429(+15)(-15)
Constant period derivative	
t_0 [BJD$_{\mathrm{TBD}}$]	2456180.558872(+22)(-21)
P [days]	1.338231502(+17)(-17)
dP/dt	$-2.74(+28)(-28) \times 10^{-10}$

[a] The numbers in parenthesis give the 68% confidence interval for the final two digits, where appropriate.

Table 4. Predicted hot Jupiter period changes from linear radial velocity trends reported by Knutson et al. (2014).

Planet	$\dot{\gamma}$ [m s^{-1} yr^{-1}]	$+\sigma_{\dot{\gamma}}$ [m s^{-1}yr^{-1}]	$-\sigma_{\dot{\gamma}}$ [m s^{-1}yr^{-1}]	P [days]	$\dot{P}_{\mathrm{RV}}$ [ms yr^{-1}]	$+\sigma_{\dot{P}_{\mathrm{RV}}}$ [ms yr^{-1}]	$-\sigma_{\dot{P}_{\mathrm{RV}}}$ [ms yr^{-1}]	Significant?
HAT-P-2 b	-0.0938	0.0067	0.0069	5.6335158	-55.62	3.97	4.09	1

NOTE— Table 4 is published in its entirety in a machine-readable format. A single row is shown here for guidance regarding form and content.